HHS Public Access

Author manuscript

Nat Mater. Author manuscript; available in PMC 2015 March 01.

Published in final edited form as:

Nat Mater. 2014 September ; 13(9): 904–911. doi:10.1038/nmat3982.

Etchable plasmonic nanoparticle probes to image and quantify cellular internalization

Gary B. Braun[1,2,*], **Tomas Friman**[1,2], **Hong-Bo Pang**[1], **Alessia Pallaoro**[3], **Tatiana Hurtado de Mendoza**[1], **Anne-Mari A. Willmore**[4], **Venkata Ramana Kotamraju**[1,2], **Aman P. Mann**[1], **Zhi-Gang She**[1], **Kazuki N. Sugahara**[1], **Norbert O. Reich**[3], **Tambet Teesalu**[1,2,4], and **Erkki Ruoslahti**[1,2,*]

[1]Cancer Research Center, Sanford-Burnham Medical Research Institute, La Jolla, CA 92037, USA

[2]Center for Nanomedicine, Sanford-Burnham Medical Research Institute at University of California, Santa Barbara, CA 93106, USA

[3]Department of Chemistry and Biochemistry, University of California, Santa Barbara, CA 93106, USA

[4]Laboratory of Cancer Biology, Institute of Biomedicine, Centre of Excellence for Translational Medicine, University of Tartu, Tartu, 50411, Estonia

Abstract

There is considerable interest in using nanoparticles as labels or to deliver drugs and other bioactive compounds to cells *in vitro* and *in vivo*. Fluorescent imaging, commonly used to study internalization and subcellular localization of nanoparticles, does not allow unequivocal distinction between cell surface-bound and internalized particles, since there is no methodology to turn particles 'off.' We have developed a simple technique to rapidly remove silver nanoparticles outside living cells leaving only the internalized pool for imaging or quantification. The silver nanoparticle (AgNP) etching is based on the sensitivity of Ag to a hexacyanoferrate/thiosulfate redox-based destain solution. In demonstration of the technique we present a new class of multicolored plasmonic nanoprobes comprising dye-labeled AgNPs that are exceptionally bright and photostable, carry peptides as model targeting ligands, can be etched rapidly and with minimal toxicity in mice and that show tumour uptake *in vivo*.

Designing nanoparticles for therapeutic, diagnostic and theranostic applications is of pivotal importance in advancing nanomedicine.[1,2] Nanoparticles (NPs) enter cultured cells at rates determined by their surface coating, size and shape.[3] Many of the clinically relevant

*Corresponding Authors: Correspondence should be addressed to: ruoslahti@sanfordburnham.org or gbraun@sanfordburnham.org.

Supporting Information: Complete experimental procedures as well as figures showing additional characterization and cell imaging.

Author Contributions: G.B.B., T.T., and E.R. initiated the research and G.B.B., H.P., T.F., A.P., T.H.dM., A.A.W, Z.S., and A.M. designed and performed experiments. K.S., T.T., N.O.R. and E.R. supervised the research. V.R.K. synthesized peptides. G.B.B. and E.R. wrote the manuscript. All authors contributed to analyzing data and revising the manuscript.

Competing financial interests: The authors declare no competing financial interests.

nanoparticle targets are intracellular and NPs are typically coated with an effector layer to engage cellular receptors and trigger internalization. Cell culture assays are used to gauge the particle binding and internalization by fluorescent, chemical, radioactive, or enzymatic tracers. Distinguishing internalized NPs from cell surface-bound particles is of pivotal importance for assessing the efficacy of NPs as targeting platforms. Disrupting ligand-receptor interactions typically involves exposing cells to low pH or using a competitive ligand, which may have unwanted effects on cell physiology and can be challenging with high-avidity NPs. Dye-labeled polymers, iron oxide, quantum dots, and gold NPs have been extensively studied as multivalent tracers, however, their removal requires harsh conditions which limits utility (e.g. dimethylformamide, strong acid, or iodine).[4-6]

Plasmonic nanomaterials made from gold (Au) and silver (Ag) are increasingly used for biological applications, particularly microscopy, stemming from their size and shape-dependent optical properties. Surface plasmons create a localized electromagnetic field, the so-called antenna effect, that leads to surface-enhanced Raman scattering (SERS) and metal-enhanced fluorescence – trackable signals that originate from molecules positioned at or near the surface, or within nanojunctions.[7-11] Of these two metals, Ag generally yields five to ten-fold more intense signals than Au,[12] which on the other hand is more commonly studied due to its chemical nobility, ease of synthesis, and distance-dependent quenching of dyes.[13] Plasmon coupling can increase both the absorption and radiative rate of dyes, while limiting photo-oxidation, dye self-quenching, and excited-state saturation.[8] The greatest enhancement is expected from AgNPs that are ∼40–100 nm in diameter,[8] a range suitable for cell targeting, however, fluorescent Ag nanoprobes that bind receptors have not yet been developed.

Here we present a nanoparticle platform that leverages the plasmonic properties of Ag to enable single particle tracking in both darkfield and fluorescence modalities, and is paired with a mild, non-permeable solution that affords the distinction between intra- and extracellularly located AgNPs through a rapid, non-toxic etching step. Our nanoparticle probe comprises a fluorescent dye-labeled polyethylene glycol (PEG) and NeutrAvidin (NA) coating around a fluorescence-enhancing AgNP core (Ag-NA). The NA serves as attachment sites for biotinylated targeting peptides, as drawn schematically in Fig. 1a. We enlisted C-end rule (CendR) peptides for proof of principle delivery into cells. CendR peptides trigger neuropilin-1 (NRP-1)-dependent cell and tissue penetration when exposed at the C-terminus of a polypeptide chain.[2,14] The Ag etching solution consists of a mixture of two chemical components (Fig. 1b) commonly used for de-staining silver-stained protein bands in polyacrylamide gels or in photographic emulsions, retasked here for etching AgNPs in a biological setting. The first etching component is a redox agent hexacyanoferrate (HCF), $Fe(III)(CN)_6^{3-}$, that oxidizes Ag^0 to Ag^+, in combination with the second component thiosulfate (TS), $S_2O_3^{2-}$, that ligates and clears away the newly formed Ag^+ ions, thereby dissolving the core (Supplementary Figs. S1-S2).[15,16] Importantly, HCF and TS are charged and do not readily diffuse through cell membranes,[17,18] thus protecting internalized AgNPs from being etched (Fig. 1). Labeled components released from etched AgNPs lose their fluorescence enhancement, further reducing the background signal.

Uptake into cells and extracellular etching were characterized using fluorescence and darkfield microscopy. CF488 dye-labeled Ag-NA carrying the prototypic CendR peptide RPARPAR (R) were visualized in NRP-1-expressing prostate cancer cells (PPC-1) before and after etching (Fig. 1c, Supplementary Fig. S3-S6).[14] The etchant selectively removed extracellular R-Ag-NA488 (those bound to the cell surface and the culture plate surface between cells), whereas the internalized fraction (appearing as yellow) were protected by the plasma membrane and remained unaltered in intensity (Fig. 1c, Supplementary Fig. S3). Darkfield imaging revealed the surviving fraction to consist of, in part, a red-shifted scattering population of Ag located in the perinuclear region of the cells (Supplementary Fig. S3). Surface plasmon oscillations, a resonant source for Rayleigh scattering, are known to plasmonically couple[8,19] when cores are within one diameter length from each other. This spectral feature can be a useful indicator of endosomal fusion and consolidation of Ag. Notably, etching of surface Ag from living cells could be accomplished in cell culture medium (Fig. 1c).

Pre-labeling the Ag-NA with dyes puts them in accord with a versatile “plug and play” targeting format used in multiplexed assays. We prepared a suite of dye-labeled Ag-NA nanoprobes to explore their use in multispectral applications, and characterized the plasmonically-driven fluorescence enhancement (EF). Metal NPs enhance the photostability and fluorescence intensity of a dye depending on i) distance from the metal surface (optimally ∼3-10 nm, or quenched if directly touching the surface),[20] ii) photophysical properties of attached dyes and labeling density, iii) spectral overlap between the plasmon resonance and dye at the wavelength of interest, and iv) the scattering efficiency of the core – which depends sensitively on composition, diameter, and shape.[8] In Fig. 2a we determined EF by etching dye-labeled samples at a constant volume, keeping the number of dyes and their concentration fixed, and comparing intensity from attached (unetched) versus the same dye free in solution (etched). The Ag-NA-dye constructs (diagrammed in Fig. 1a with peptides) were ∼5 to 15 fold brighter prior to etching, indicating that dyes are enhanced by the local field around 70 nm Ag-NA. This held true for a range of dyes from ultraviolet to near-infrared (NIR) (Fig. 2a, Supplementary Fig. S7). In contrast, we found that smaller Ag-NA (20 nm, with a similar coating) gave EF values of ∼1, consistent with the predicted 40 nm diameter threshold for enhancement. The cyanine dyes Cy3, CF555, and DL550 showed the largest EFs, 12 ± 2 (Fig. 2a, Supplementary Fig. S7) for 70 nm Ag-NA, consistent with an EF of 12 previously reported using Ag islands on quartz films coated with Cy3- and Cy5-labeled albumin.[20] While the current Ag-NA design establishes a broad spectral range on a rapidly etched (Fig. 2b) single core platform, we anticipate that EF in the NIR range could be improved by a judicious tuning of the plasmonic spectral envelope (Supplementary Fig. S1), for example, by using non-spherical Ag cores which are known to exhibit NIR to IR resonance.[7]

To develop a set of etching techniques we evaluated the toxicity of this etchant in cell cultures and *in vivo* with mice. Long-term cell viability was not affected by AgNPs or their etching, but decreased if continuously exposed to high etchant concentrations for 24 h (Fig. 2c, Supplementary Fig. S4). The etchant combination is thus mild, and selective, since AuNPs could not be dissolved owing to their higher reduction potential (Supplementary Fig.

S5).[6,21] In addition, it is known that the anti-oxidant ascorbate can reduce HCF and we confirmed that etchant activity is rapidly quenched (Supplementary Fig. S5), a feature which could enable pulse-chase experimental formats.[22] Clinical blood chemistry analysis of mice injected with Ag-NA or the etchant showed normal hepatic and kidney function as measured, for example, by analysis of alanine aminotransaminase, amylase, and blood urea nitrogen levels, indicating the general safety of both Ag-NA[23] and etchant[18,32,33] in cell and tumor homing studies (Fig. 2d, Supplementary Fig. S4). However, detailed studies may be needed to further explore the potential toxicity. Importantly, the concentration of etchant we tested was sufficient to etch AgNPs in blood (Fig. 2e).

We evaluated the performance of etchable dye-labeled Ag in flow cytometry. Flow cytometry is a well-established quantitative method for fluorescent detection of cells that has not yet been used with fluorescent Ag probes, yet should benefit from their expectedly high radiative rate and saturation limit.[20,24] Ag-NA with Alexa Fluor 647 dye were loaded with either RPARPAR (R-Ag-NA647) or RPARPARA (RA-Ag-NA647), a C-terminally blocked control peptide that has negligible affinity to NRP-1.[25,26] A plus/minus etch strategy was implemented with the aim of quantifying the specific internalization of NPs. Cells were first incubated with R-Ag-NA647 or RA-Ag-NA647 and then each sample was split into two parts – one of which was etched to remove the non-internalized fraction (Fig. 3a). Using flow cytometry we found that the forward scatter (FSC) typically used as an indicator of cell size was insensitive to Ag-NA647. We therefore chose FSC to gate for cells (applied in Fig. 3b). We then compared signals from etched and unetched samples and calculated the internalized fraction by the mean intensity ratio. Approximately 60% of the fluorescence signal from R-Ag-NA647 was not etchable (i.e. ∼60% internalized) after 1 h of incubation with cells. Functionalized with the control peptide, RA-Ag-NA647 showed only weak binding with complete etchability (∼1% internalized, Fig. 3b, c), consistent with the receptor-binding motif being crucial for internalization. Robust internalization and etch-protection using the peptide RPARPAR was further corroborated by darkfield scattering from R-Ag-NA647 inside suspended cells (Fig. 3d).

We found that, unlike most probes commonly used in flow cytometry, binding by Ag-NA647 dramatically altered the side scatter (SSC) signal from cells, and the effect was proportional to the fluorescence signal across a wide dynamic range (Fig. 3d,e). Cells without Ag-NA647 did not show this behavior (black). The basis for increased SSC is likely the intense resonant AgNP plasmon scattering light at the 488 nm laser wavelength[7] (Fig. 3b, Supplementary S2-3). Post-etch dot plots showed a disappearance of low-signal events in both SSC and fluorescence, additional evidence that non-internalized Ag-NA647 were removed (Fig. 3e). Generalizing these results, AgNP SSC could be monitored in label-free uptake assays, or as a confirmatory or ratiometric reference signal, e.g. when using pH-sensitive dyes. The proportionality we observe between SSC and fluorescence indicates uniform dye labeling as well as a minimal change of AF647 fluorescence following endocytosis. These results provide a blueprint for the design and use of AgNPs for flow cytometry applications.

Imaging of probes in live cells is particularly demanding, as it requires a material to be both bright and photostable. To explore such applications we prepared CF555 dye-labeled 70 nm

R-Ag-NA555 and allowed them to internalize into NRP-1 expressing GFP-PC-3 (prostate cancer) cells (Fig. 4). These cells have cytosolic GFP and were chosen to allow distinction to be made between R-Ag-NA555 adsorbed between cells (red) and those inside the cell (yellow overlay). Etching specifically reduced the membrane-bound as well as plate-adsorbed R-Ag-NA555 (Fig. 4a, Supplementary Movie S8). At a lower dose R-Ag-NA555 was easily tracked as NPs that moved in relation to each another inside cells (Fig. 4b). Due to the large (>1 μm) separation, the Ag were presumably contained in separate endosomes. Their convergence into a single spot was therefore most likely an endosome fusion event, as we found no subsequent separation over 25 min. These results show that dye-labeled Ag nanoprobes can be tracked through the cell uptake and intracellular transport process.

We found that aldehyde-fixed GFP-PC-3 cells remained protective over the endocytosed R-Ag-NA555, since particles near the center of the cells were not removed by etchant (Fig. 4d). Disrupting the membrane of fixed and etched cells by adding the detergent Triton X-100, in the presence of etchant, quickly diminished the remaining fluorescent regions (Fig. 4d,e). Presumably, this resilience was due to the stability of lipid bilayers that exclude HCF or TS.[17] The permeability data adds further support to the proposed mechanism that impermeable membranes are the critical factor shielding Ag from the highly charged etchant molecules.

The potential of Ag in multiplexed microscopy was tested with cells and tissues (Fig. 5). We prepared both green and red dye-labeled 70 nm Ag-NA, mixed and physically filtered them (0.22 μm), and deposited on a glass slide. Dye-labeled Ag-NA were bright enough and sufficiently separated from one another to be visualized individually in their respective fluorescent channels and in darkfield,[27] despite their small size (Fig. 5a). We next coated the red and green Ag-NA with two different peptides that bind to different receptors, and incubated them with PPC-1 cells.[28] The observed heterogeneous binding pattern of green and red fluorescent Ag-NA indicates a capacity for differential targeting and multiplexing (Fig. 5b). We also explored smaller size Ag-NA in the context of imaging, and for uptake pathway studies. Antibody staining with anti-NRP-1 on fixed cells showed colocalization with 20 nm RPARPAR Ag-NA555 (Fig. 5c, not etched) demonstrating that smaller 20 nm Ag-NA are viable as photostable targeted nanoprobes, despite their being less bright than the larger Ag.

We evaluated the use of AgNPs with living three-dimensional (3D) ‘organotypic’ tumor slices. These cultures preserve the complex tumor tissue architecture and the epithelial-stromal interactions, important considerations in drug delivery and tissue transport studies.[29] We used a tumor penetrating peptide iRGD, with sequence [CRGDKGPDC]. iRGD binds integrins overexpressed in many types of tumors and is proteolytically processed into a CendR peptide, that then internalizes into cells.[25,30] Tissue penetration of iRGD-Ag-NA647 (70 nm) was readily visualized by post-etch mapping in 3D using confocal microscopy, revealing localized hot spots of endocytosis (Fig. 5d, e) that were not found using control particles.

Injected therapeutic NPs follow a path that can be broken down to three major steps: circulation, binding, and internalization. Extravasation occurs as NPs pass from blood into

tissue by passive leakage or endocytosis,[31] and these contributions sum to give the signal and contrast seen with “always-on” imaging probes. Endocytosis by cells is challenging to detect, but is of great interest for delivery of membrane-impermeable drugs (e.g. nucleic acids) that act against intracellular targets. To test if etchable NPs can provide internalization contrast, we injected iRGD-Ag-NA into circulation in mice bearing the 4T1 breast cancer tumors. After perfusion to remove unbound NPs from the vasculature, we etched tissue sections from both tumor and liver (Fig. 6a). The spatial pattern of Ag in the tumor (Fig. 6b) was found to dramatically change upon etching, showing loss of the diffuse signal and revealing an underlying punctate pattern reminiscent of the *in vitro* result in Fig. 4a,d. By comparing + and no etch we estimated the degree of Ag internalization into the tumor cells to be ∼25% (Fig. 6c). This result was compared to liver internalization (∼100% Fig. 6b,c), that can be attributed to internalization by liver-resident macrophages known to rapidly capture circulating NPs.

Injecting etchant into mice previously injected with AgNPs cleared the blood of circulating AgNPs (Fig. 2c). In light of this finding, and considering the small size of the etchant molecules, we explored the possibility that AgNPs trapped in the extravascular/extracellular space may also be etched. Indeed, the components TS and HCF are known to distribute through tissues without crossing membranes,[18,32,33] and have been used to estimate the extracellular fluid volume in mammals.[18,32] Furthermore, the reaction products comprise stable and soluble compounds (Fig. 1b) that should not interfere with the autometallography used to amplify Ag signal for histological analysis.

We developed an *in vivo* etching strategy that gives circulating NPs a set amount of time to find their target before chasing with an intravenous bolus of etchant (Fig. 6a, lower pathway). Comparing +/- etchant would then discriminate between accumulation in the tumor (homing) and internalization by cells within the tumor (i.e. cell uptake). A possible complication for etching is that parts of the tumor can have dysfunctional local vasculature, impairing delivery,[34] however, those regions might also receive fewer AgNPs. We chose the well-studied MMTV-PyMT transgenic mouse model that has relevance to human breast cancer, particularly the stages of its progression.[35] The Ag nanoprobe was modified to carry polyethylene glycol (PEG)-linked iRGD, instead of NA linked with biotin iRGD, to more closely resemble therapeutic “stealth” NPs, and to allow repeat injections in an immunocompetent setting.[36] iRGD is a tumor-specific homing peptide that is converted into a CendR peptide in tumors. It has been found to increase tumor homing and extravasation of NPs in several breast cancer models.[25,37]

Tumor-bearing MMTV-PyMT mice injected with iRGD-Ag-PEG displayed a heterogeneous homing pattern in the tumor (Fig. 6d,e, 4 h, –etch condition), similar to Fig. 6b and other NP homing studies.[25,28] Quantifying Ag pixels showed an initial homing burst (0.5 h, no etch), followed by a doubling between 0.5 h and 4 h, and doubling again by 24 h circulation time (Fig. 6f). Clearance by the reticuloendothelial system of circulating NPs could explain the decreased homing rate. Notably, relative to non-etched counterparts, mice that received an injection of etchant had a diminished quantity of Ag, irrespective of circulation time for iRGD-Ag-PEG. Assuming the Ag pixels from etched samples were due to the cell-internalized NPs, we may conclude the following: a significant amount of iRGD-Ag-PEG

internalized as early as 0.5 h (Fig. 6f, +etch), and increased four-fold by 24 h (+etch). The rate of internalization paralleled the rate of Ag homing (no etch, 24 h). Comparing +etch and no etch we estimate ∼30% of the homing resulted with internalization by 24 h, similar to the ex vivo tumor result in Fig. 6c (∼25%, 24 h). Together, these data suggest a new method to determine intracellular biodistribution kinetics that uses etchable AgNPs as a model nanosystem for targeted therapeutics.

AgNP probes combine traits of etchability and brightness, in both fluorescence and scattering imaging modalities, with spectral barcoding, photostability, and sensitivity to the single particle level. The AgNPs were functionalized with NeutrAvidin for facile loading of affinity tags, and imaged inside cancer cells *in vitro* and *in vivo*. AgNPs also seem particularly promising for flow cytometry, which was implemented here to more finely parse receptor specificity and uptake efficiency. As other virus-like particles, AgNPs can carry a multiplicity of ligands that increase their avidity – short peptides, employed in this work, are of particular interest due to their specificity and minimal immunogenicity, however, antibody or aptamer[38] targeting elements may be conjugated to AgNPs. Coatings that respond to an electrochemical cue by a shape-change are also possible, including Au-Ag,[39-41] redox-sensitive cleavable linkers,[39,42] and biomolecular nanostructures.[43-45] Multiplexed detection of internalized Ag should lead to a better understanding of NP-cell interactions and the role of size, shape, and coating during molecular transport through tissue and cells. The recent emergence of NIR and multi-photon excitation systems for *in vivo* mapping provide key design features for engineering the inherently non-linear optical properties of plasmonic nanoparticles. Taken together, these results illustrate how plasmonic nanoprobes based on etchable Ag cores will be a powerful tool in studies of targeted uptake and trafficking from a subcellular to tissue level.

Methods Summary

Materials

Ag nanoparticles were synthesized and coated as described in the Supplementary Information. Coatings around Ag were based on either NeutrAvidin (Ag-NA) protein or PEG-maleimide (Ag-PEG). Amine-reactive dyes were attached to NA nanoparticles for fluorescence microscopy and FACS (e.g. Ag-NA488). Peptides were synthesized with a biotin label for loading into the binding pocket of NA. Free cysteine-containing peptides were prepared as previously described and conjugated to PEG-maleimide.[14,25] The etchant was composed of tripotassium hexacyanoferrate (HCF) and sodium thiosulfate pentahydrate (TS) (Sigma), working concentration of 1-10 mM HCF and TS.

In vitro imaging

Cell imaging experiments were performed in culture plates or glass bottom reservoirs as described in Supporting Information. Typically, biotin-X-RPARPAR-OH was attached to dye-labeled nanoparticles (e.g. R-Ag-NA488) and added to PPC-1 or PC3-GFP prostate cancer cells in DMEM culture medium with 10% FBS. In some experiments, cells were washed with Hanks buffered saline solution (HBSS, Hyclone). Addition of etchant solution to the medium removed extracellular Ag. Where indicated, nuclear stain Hoescht

(Invitrogen) was added to the media prior to epifluorescence imaging. Antibodies used were against NRP-1 (Novus), and Alexa Fluor 488 anti-Rabbit secondary antibody (Invitrogen).

Flow cytometery

PPC-1 cells were suspended in DMEM with 10 μM t-RNA. Ag-NA647, carrying either biotin-X-RPARPAR-OH (R) or biotin-X-RPARPARA-OH (RA), was incubated with cells for 1 h. Etchant in PBS was added to specified samples, followed by centrifugation and resuspension in media. Analysis was performed on a BD Accuri C6 Flow Cytometer.

Ex vivo tissue penetration assay

All animal work was approved by the Institutional Animal Care Committee of the Sanford Burnham Medical Research Institute. MCF10CA1a human breast cancer cells were inoculated in nude female mice and grown to ∼1 cm diameter. Tumors were excised and sliced with a Leica VT1200 vibratome at a thickness of ∼400 μm and cultured overnight. The next day the tumor slices were incubated with nanoparticles for 2 hours at 37 °C, washed with PBS, exposed for 1 min to etchant in PBS, washed, fixed, permeabilized, DAPI stained, and mounted (ProLong). Confocal microscopy (Olympus) Z-stacks were rendered in 3D perspective. Nanoparticles: Ag-NA647 with biotin-X-GGSGGSGG-[CRGDKGPDC]-NH_2 (iRGD-Ag-NA647), where X = aminohexanoic linker and the two cysteine residues were disulfide bonded, or Ag-NA647 with D-biotin (control).

Etching kinetics

Kinetics etching data was collected using a fluorimeter (Horiba) monitoring 90° scattering signal from 70 nm Ag-NA in solution. Excitation and emission were set at 470 nm and 520 nm with 5 nm slit widths. Scattering signal dropped upon adding the etchant. The slope was fit using a linear function and converted to an etch rate in units of percent of initial signal per second. The time at which signal was 10% of initial intensity was plotted by manual examination of the raw data. Etchant reagent stoichiometry was 1:1 unless otherwise specified and Ag-NA concentration was fixed for all experiments.

In vivo homing with *ex vivo* etching

For in vivo homing experiments 25-50 nm iRGD-Ag-NA was injected by tail vein. Mice were perfused at 24 h under deep anesthesia (Avertin) and tissues were frozen in liquid nitrogen. Cryosections were prepared and fixed in 4% paraformaldehyde in PBS. Etchant was applied for 5 s followed by PBS and then water. Aldehyde was blocked and cells permeabilized in a glycine blocking solution. LI Silver Enhancement kit (Molecular Probes) was used to amplify Ag signals, and coverslipped. Brightfield images were quantified with ImageJ software (NIH).

In vivo homing and etching

iRGD-Ag-PEG synthesis is described in Supporting Information. Briefly, Ag-PEG-NH_2 was backfilled using the peptide Ac-CCPGCC-NH_2 (Lifetein, Inc.). A linker molecule NHS-PEG-Maleimide was attached (5 kDa, Jenkem USA),[28] followed by coupling FAM-cys-X-[CRGDKGPDC]-NH_2 as in ref.[25] FAM is fluorescein, X = aminohexanoic linker, and

brackets indicate disulfide bond in iRGD between the two C residues. The sodium salt of HCF was prepared by sodium ion exchange resin treatment of 0.2 M $K_3Fe(CN)_6$ solution. Sodium-HCF was combined with 0.2 M $Na_2S_2O_3$ and 1 M NaCl to prepare ~150 mM Na^+, 17 mM $Fe(CN)_6^{3-}$, and 50 mM $S_2O_3^{2-}$ as the etchant. MMTV-PyMT tumor-bearing mice were injected with iRGD-Ag-PEG, and at a specified time later with etchant, both by tail vein. Tissue sections were fixed, blocked, permeabilized, and Ag amplified as above. Nuclei were stained using Nuclear Fast Red (Sigma), dehydrated, and mounted (DPX, Sigma). Aperio ScanScope XT scanner and ImageJ were used to image and quantify brown-black as positive Ag pixels per field. For darkfield imaging, samples without nuclear stain were imaged using a Leica DM-IRE2.

Statistical analysis

Values are reported as mean ± S.D. unless otherwise specified. Statistical analysis was performed with GraphPad Prism using two-way analysis of variance.

Supplementary Material

Refer to Web version on PubMed Central for supplementary material.

Acknowledgments

This work was supported by US DoD awards W81XWH-10-1-0199, and W81XWH-09-0698, R01 CA152327, R01 CA167174, and CA 030199 (Cancer Center Support grant) from the NCI, and by the Defense Advanced Research Projects Agency (DARPA) under Cooperative Agreement HR0011-13-2-0017. The content of the information within this document does not necessarily reflect the position or the policy of the Government. G.B.B. was supported by the Cancer Center of Santa Barbara and by an NIH training grant (T32 CA121949), and A.M.W, and T.T. by the European Research Council under the European Union's Seventh Framework Programme (FP/2007-2013)/ERC Starting Grant Agreement No. 291910. The authors thank L. Agemy, R. Chen, and M. Moskovits for helpful discussions, A. Kylander-Clark for assistance and technical support with ICP-MS, F. Zhang for guidance in Ag synthesis, F. Vitti for helpful discussions on silver amplification, J. Wang for flow cytometry assistance, the NRI-MCDB Microscopy Facility at UCSB, and Histology and Cellular Imaging cores at the Sanford-Burnham Medical Research Institute.

References

1. Tassa C, Shaw SY, Weissleder R. Dextran-coated iron oxide nanoparticles: a versatile platform for targeted molecular imaging, molecular diagnostics, and therapy. Accounts of chemical research. 2011; 44:842–852.10.1021/ar200084x [PubMed: 21661727]
2. Ruoslahti E. Peptides as Targeting Elements and Tissue Penetration Devices for Nanoparticles. Adv Mater. 201210.1002/adma.201200454
3. Chithrani BD, Chan WC. Elucidating the mechanism of cellular uptake and removal of protein-coated gold nanoparticles of different sizes and shapes. Nano letters. 2007; 7:1542–1550.10.1021/nl070363y [PubMed: 17465586]
4. Goulet PJ, Bourret GR, Lennox RB. Facile phase transfer of large, water-soluble metal nanoparticles to nonpolar solvents. Langmuir : the ACS journal of surfaces and colloids. 2012; 28:2909–2913.10.1021/la2038894 [PubMed: 22283327]
5. Moller J, et al. Dissolution of iron oxide nanoparticles inside polymer nanocapsules. Physical chemistry chemical physics : PCCP. 2011; 13:20354–20360.10.1039/c1cp22161b [PubMed: 21993837]
6. Cho EC, Xie J, Wurm PA, Xia Y. Understanding the role of surface charges in cellular adsorption versus internalization by selectively removing gold nanoparticles on the cell surface with a I2/KI etchant. Nano letters. 2009; 9:1080–1084.10.1021/nl803487r [PubMed: 19199477]

7. Sun Y, Xia Y. Gold and silver nanoparticles: a class of chromophores with colors tunable in the range from 400 to 750 nm. The Analyst. 2003; 128:686–691. [PubMed: 12866889]
8. Lakowicz JR. Radiative decay engineering 5: metal-enhanced fluorescence and plasmon emission. Analytical biochemistry. 2005; 337:171–194.10.1016/j.ab.2004.11.026 [PubMed: 15691498]
9. Zhang F, et al. Fabrication of Ag@SiO(2)@Y(2)O(3):Er nanostructures for bioimaging: tuning of the upconversion fluorescence with silver nanoparticles. Journal of the American Chemical Society. 2010; 132:2850–2851.10.1021/ja909108x [PubMed: 20158187]
10. Mulvihill MJ, Ling XY, Henzie J, Yang P. Anisotropic etching of silver nanoparticles for plasmonic structures capable of single-particle SERS. Journal of the American Chemical Society. 2010; 132:268–274.10.1021/ja906954f [PubMed: 20000421]
11. Braun GB, et al. Generalized Approach to SERS-Active Nanomaterials via Controlled Nanoparticle Linking, Polymer Encapsulation, and Small-Molecule Infusion. Journal of Physical Chemistry C. 2009; 113:13622–13629.10.1021/Jp903399p
12. Bharadwaj P, Novotny L. Spectral dependence of single molecule fluorescence enhancement. Opt Express. 2007; 15:14266–14274. [PubMed: 19550702]
13. Kim JH, Estabrook RA, Braun G, Lee BR, Reich NO. Specific and sensitive detection of nucleic acids and RNases using gold nanoparticle-RNA-fluorescent dye conjugates. Chem Commun (Camb). 2007:4342–4344.10.1039/b710306a [PubMed: 17957280]
14. Teesalu T, Sugahara KN, Kotamraju VR, Ruoslahti E. C-end rule peptides mediate neuropilin-1-dependent cell, vascular, and tissue penetration. Proceedings of the National Academy of Sciences of the United States of America. 2009; 106:16157–16162.10.1073/pnas.0908201106 [PubMed: 19805273]
15. Meywald T, Scherthan H, Nagl W. Increased specificity of colloidal silver staining by means of chemical attenuation. Hereditas. 1996; 124:63–70.10.1111/j.1601-5223.1996.00063.x [PubMed: 8690615]
16. Scheler C, et al. Peptide mass fingerprint sequence coverage from differently stained proteins on two-dimensional electrophoresis patterns by matrix assisted laser desorption/ionization-mass spectrometry (MALDI-MS). Electrophoresis. 1998; 19:918–927.10.1002/elps.1150190607 [PubMed: 9638938]
17. Koley D, Bard AJ. Triton X-100 concentration effects on membrane permeability of a single HeLa cell by scanning electrochemical microscopy (SECM). Proceedings of the National Academy of Sciences of the United States of America. 2010; 107:16783–16787.10.1073/pnas.1011614107 [PubMed: 20837548]
18. Cardozo RH, Edelman IS, Moore FD. Sodium thiosulfate dilution as a measure of the volume of fluid outside of body cells. Surgical forum. 1951:606–611. [PubMed: 14931297]
19. Liu N, Hentschel M, Weiss T, Alivisatos AP, Giessen H. Three-dimensional plasmon rulers. Science. 2011; 332:1407–1410.10.1126/science.1199958 [PubMed: 21680838]
20. Malicka J, Gryczynski I, Gryczynski Z, Lakowicz JR. Effects of fluorophore-to-silver distance on the emission of cyanine-dye-labeled oligonucleotides. Analytical biochemistry. 2003; 315:57–66. [PubMed: 12672412]
21. Burdinski D, Blees MH. Thiosulfate- and thiosulfonate-based etchants for the patterning of gold using microcontact printing. Chemistry of Materials. 2007; 19:3933–3944.10.1021/Cm070864k
22. Van Duijn MM. Ascorbate Stimulates Ferricyanide Reduction in HL-60 Cells through a Mechanism Distinct from the NADH-dependent Plasma Membrane Reductase. Journal of Biological Chemistry. 1998; 273:13415–13420.10.1074/jbc.273.22.13415 [PubMed: 9593673]
23. De Jong WH, et al. Systemic and immunotoxicity of silver nanoparticles in an intravenous 28 days repeated dose toxicity study in rats. Biomaterials. 2013; 34:8333–8343.10.1016/j.biomaterials.2013.06.048 [PubMed: 23886731]
24. Lakowicz JR, et al. Radiative decay engineering. 2. Effects of Silver Island films on fluorescence intensity, lifetimes, and resonance energy transfer. Analytical biochemistry. 2002; 301:261–277.10.1006/abio.2001.5503 [PubMed: 11814297]
25. Sugahara KN, et al. Tissue-penetrating delivery of compounds and nanoparticles into tumors. Cancer cell. 2009; 16:510–520.10.1016/j.ccr.2009.10.013 [PubMed: 19962669]

26. Teesalu T, Sugahara KN, Ruoslahti E. Mapping of vascular ZIP codes by phage display. Methods in enzymology. 2012; 503:35–56.10.1016/B978-0-12-396962-0.00002-1 [PubMed: 22230564]
27. McFarland AD, Van Duyne RP. Single Silver Nanoparticles as Real-Time Optical Sensors with Zeptomole Sensitivity. Nano letters. 2003; 3:1057–1062.10.1021/nl034372s
28. Roth L, et al. Transtumoral targeting enabled by a novel neuropilin-binding peptide. Oncogene. 201110.1038/onc.2011.537
29. Vaira V, et al. Preclinical model of organotypic culture for pharmacodynamic profiling of human tumors. Proceedings of the National Academy of Sciences of the United States of America. 2010; 107:8352–8356.10.1073/pnas.0907676107 [PubMed: 20404174]
30. Chen R, et al. Application of a proapoptotic peptide to intratumorally spreading cancer therapy. Cancer Res. 2013; 73:1352–1361.10.1158/0008-5472.CAN-12-1979 [PubMed: 23248118]
31. Ruoslahti E, Bhatia SN, Sailor MJ. Targeting of drugs and nanoparticles to tumors. The Journal of cell biology. 2010; 188:759–768.10.1083/jcb.200910104 [PubMed: 20231381]
32. Zweens J, Frankena H, Rispens P, Zijlstra WG. Determination of extracellular fluid volume in the dog with ferrocyanide. Pflugers Arch. 1975; 357:275–290.10.1007/BF00585982 [PubMed: 1105397]
33. Mendel B. The Action of Ferricyanide on Tumour Cells. The American Journal of Cancer. 1937; 30:549–552.10.1158/ajc.1937.549
34. Gillies RJ, Schornack PA, Secomb TW, Raghunand N. Causes and effects of heterogeneous perfusion in tumors. Neoplasia. 1999; 1:197–207. [PubMed: 10935474]
35. Lin EY, et al. Progression to malignancy in the polyoma middle T oncoprotein mouse breast cancer model provides a reliable model for human diseases. The American journal of pathology. 2003; 163:2113–2126.10.1016/S0002-9440(10)63568-7 [PubMed: 14578209]
36. Agemy L, et al. Targeted nanoparticle enhanced proapoptotic peptide as potential therapy for glioblastoma. Proceedings of the National Academy of Sciences of the United States of America. 2011; 108:17450–17455.10.1073/pnas.1114518108 [PubMed: 21969599]
37. Sugahara KN, et al. Coadministration of a tumor-penetrating peptide enhances the efficacy of cancer drugs. Science. 2010; 328:1031–1035.10.1126/science.1183057 [PubMed: 20378772]
38. Farokhzad OC, et al. Targeted nanoparticle-aptamer bioconjugates for cancer chemotherapy in vivo. Proceedings of the National Academy of Sciences of the United States of America. 2006; 103:6315–6320.10.1073/pnas.0601755103 [PubMed: 16606824]
39. Chuntonov L, Bar-Sadan M, Houben L, Haran G. Correlating electron tomography and plasmon spectroscopy of single noble metal core-shell nanoparticles. Nano letters. 2012; 12:145–150.10.1021/nl204125d [PubMed: 22168793]
40. Gu H, Yang Z, Gao J, Chang CK, Xu B. Heterodimers of Nanoparticles: Formation at a Liquid–Liquid Interface and Particle-Specific Surface Modification by Functional Molecules. Journal of the American Chemical Society. 2005; 127:34–35.10.1021/ja045220h [PubMed: 15631435]
41. Pallaoro A, Braun GB, Moskovits M. Quantitative ratiometric discrimination between noncancerous and cancerous prostate cells based on neuropilin-1 overexpression. Proceedings of the National Academy of Sciences of the United States of America. 2011; 108:16559–16564.10.1073/pnas.1109490108 [PubMed: 21930955]
42. Uozumi J, Ishizawa M, Iwamoto Y, Baba T. Sodium thiosulfate inhibits cis-diamminedichloroplatinum (II) activity. Cancer chemotherapy and pharmacology. 1984; 13:82–85. [PubMed: 6540631]
43. Koyfman AY, et al. Controlled spacing of cationic gold nanoparticles by nanocrown RNA. Journal of the American Chemical Society. 2005; 127:11886–11887.10.1021/ja051144m [PubMed: 16117496]
44. Koyfman AY, Braun GB, Reich NO. Cell-targeted self-assembled DNA nanostructures. Journal of the American Chemical Society. 2009; 131:14237–14239.10.1021/ja9015638 [PubMed: 19754205]
45. Idili A, Plaxco KW, Vallee-Belisle A, Ricci F. Thermodynamic basis for engineering high-affinity, high-specificity binding-induced DNA clamp nanoswitches. ACS nano. 2013; 7:10863–10869.10.1021/nn404305e [PubMed: 24219761]

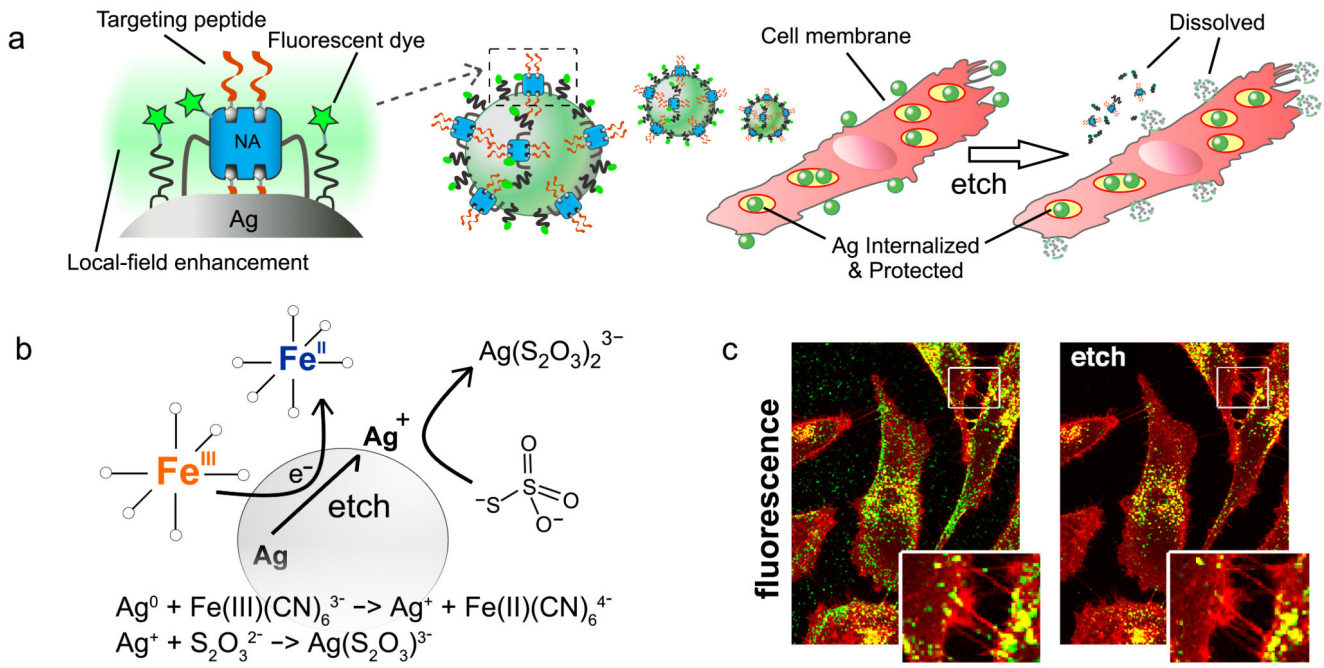

Figure 1. Dye-labeled, peptide functionalized silver nanoparticles (AgNPs) and their etching for cell internalization and tracking

(a) Scheme of AgNPs coated with NeutrAvidin-PEG-thiol (NA) and lipoic-PEG-amine, each having attached fluorescent dyes (stars) with brightness enhanced by the local plasmonic field. Attachment of biotinylated internalizing peptide RPARPAR forms the complete Ag nanoprobe (R-Ag-NA488). These bind to and are taken up by cells, which are treated with exposure to etchant solution to remove extracellular particles. Plasmonic enhancement is lost for etched particles. (b) Etching reagents hexacyanoferrate (HCF) and thiosulfate (TS) oxidize and stabilize silver ions, respectively, releasing components into solution and dissolving the core. (c) Fluorescence confocal microscopy of cells incubated with R-Ag-NA488 (green) and membrane stain (red) shows how R-Ag-NA488 is retained selectively in cells when etched (right). Endosomal membranes strongly overlap with nanoparticles, appearing as yellow in the overlay.

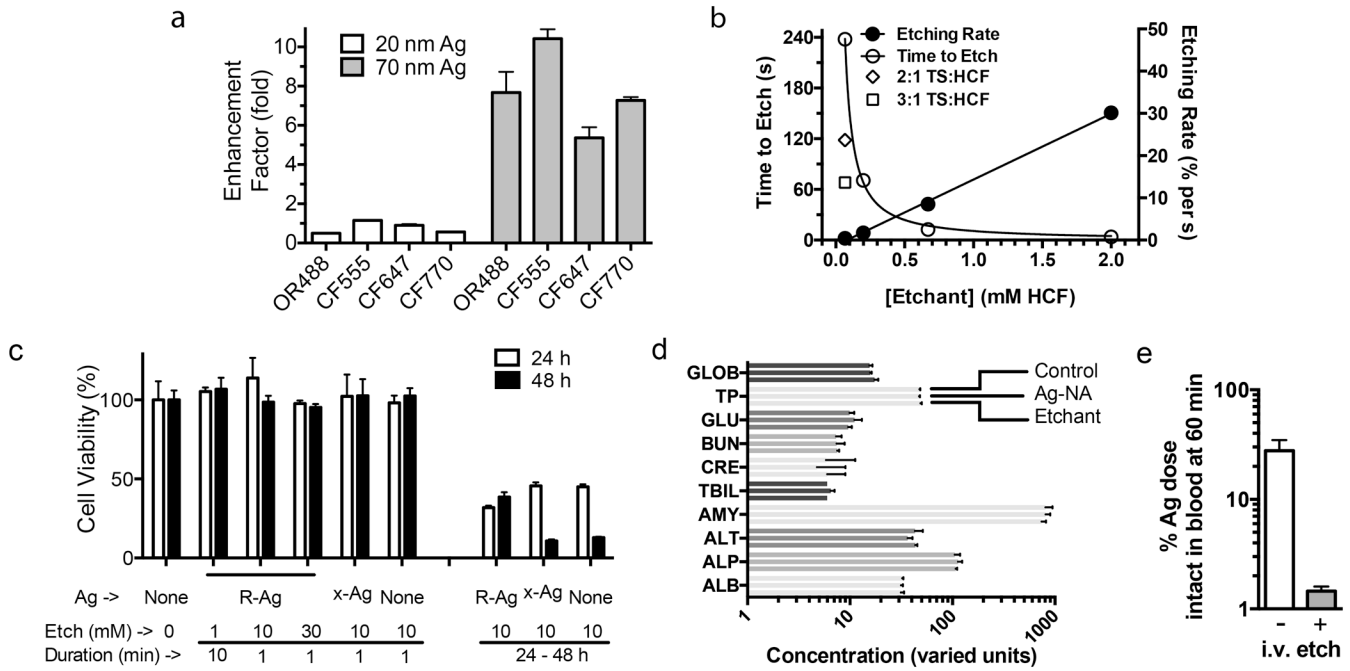

Figure 2. Nanoparticle characterization and toxicity screening

(a) Enhancement factor (EF) for several commonly used dyes shows a strong dependence for size of the Ag core. EF was calculated from the ratio of fluorescence for unetched/etched Ag-NA-dye conjugates. The approximate peak absorption value of the dye is on the x-axis. Error bars = S.D. from replicate wells. OR488, Oregon Green 488; CF dyes from Biotium. (b) Etching kinetics for Ag-NA depends linearly on the concentration and the molar ratio of the etchant components TS:HCF. The decrease in scattering intensity from the Ag plasmon band upon etching was used to calculate a rate, and the time to reach 10% of the initial value is plotted. 1:1 TS:HCF except where indicated, Ag-NA (70 nm core) concentration fixed in all conditions. (c) PPC-1 cells with RPARPAR Ag-NA (R-Ag) and etching showed no effect on 48 h viability (resazurin assay) for short-term exposures to etchant. N=6. Values normalized to the condition of no Ag, no etchant. Ag-NA without peptide, x-Ag, does not internalize into cells. Etchant concentration and duration of contact with cells is indicated. (d) In vivo blood chemistry was evaluated 24 h after x-Ag-NA or etchant injection. Marker levels were not significantly different from those for a PBS control injection, see Supporting Information for additional plots. Error bars = S.D. N=3-6 mice. (e) The etchant was capable of etching pre-injected Ag in mice. Ag was injected into the tail vein then 20 min later followed by either etchant or PBS injection, and blood was analyzed for fluorescence at 60 min. Values were normalized to % of fluorescence at 5 min. Ag had been labeled with CF555 and PEG for blood etching, see Supporting Information. Error bars = S.D., N=2. Terms and units for d: GLOB, globulin g/L; TP, total protein g/L; GLU, glucose mM; BUN, blood urea nitrogen mM; CRE, creatinine μM; TBIL, total bilirubin μM; AMY, amylase units/L; ALT, alanine transaminase units/L; ALP, alkaline phosphatase units/L; ALB, albumin g/L.

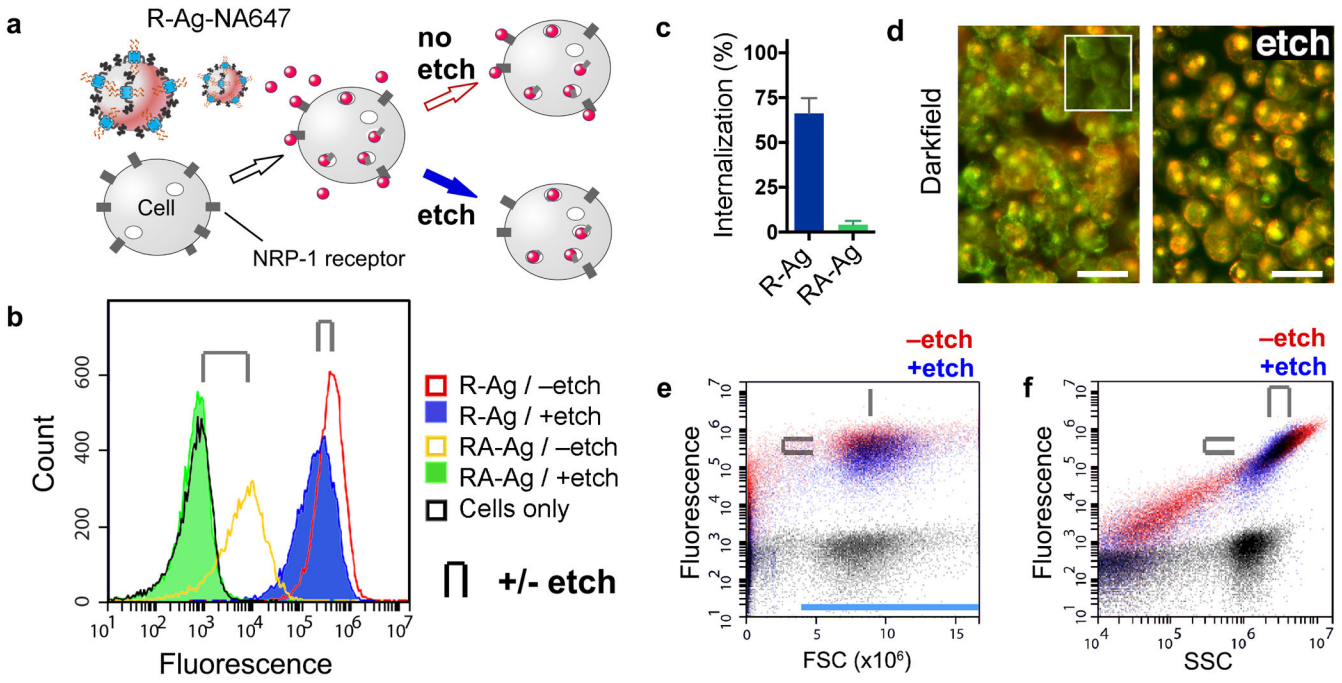

Figure 3. Flow cytometry with AgNPs

(a) Scheme of CendR peptide RPARPAR dependent R-Ag-NA647 binding to NRP-1 expressing cells. After splitting into two samples one is etched. (b) Fluorescence histograms of cells with Ag-NA647 carrying either of two peptides. Cell-gated plots of internalizing R-Ag-NA647 (red, -etch), and with etch (blue), versus non-internalizing control, RPARPARA (RA)-Ag-NA647 (yellow, -etch) and with etch (green). Cells without Ag were included as a control (black). Paired +/- etch is indicated in all panels by the clip icon. (c) Internalization into cells was quantified from b as the percent of mean signal retained after etching. Error bars (S.D.) were generated across five separate incubations and cytometric runs. (d) Darkfield imaging of cell suspensions with R-Ag-NA647 shows that etched cells lose the membrane puncta (Ag) but retain the perinuclear (and red-shifted) scattering spectra from internalized Ag. Inset shows cells without AgNPs. Scale bars are 25 μm. (e) R-Ag-NA647 from b plotted as ungated dot plots in fluorescence versus forward scatter (FSC) or (panel f) side scatter (SSC). Black dot plots are from cells-only control. In e, FSC detected cells but the signal did not shift when cells were bound with R-Ag-NA647; only y-axis fluorescence shifts were observed. FSC thus served as a stable gate parameter, indicated by the blue bar, and was used for creating panel b. In f, both SSC and fluorescence increased due to R-Ag-NA647 (red). Etching caused a slight loss in signal from cells (upper-right population), attributed to the etching away of membrane-bound Ag, and a loss of events below the cell-minimum SSC at ~10^6 counts was attributed to free R-Ag-NA647 or debris.

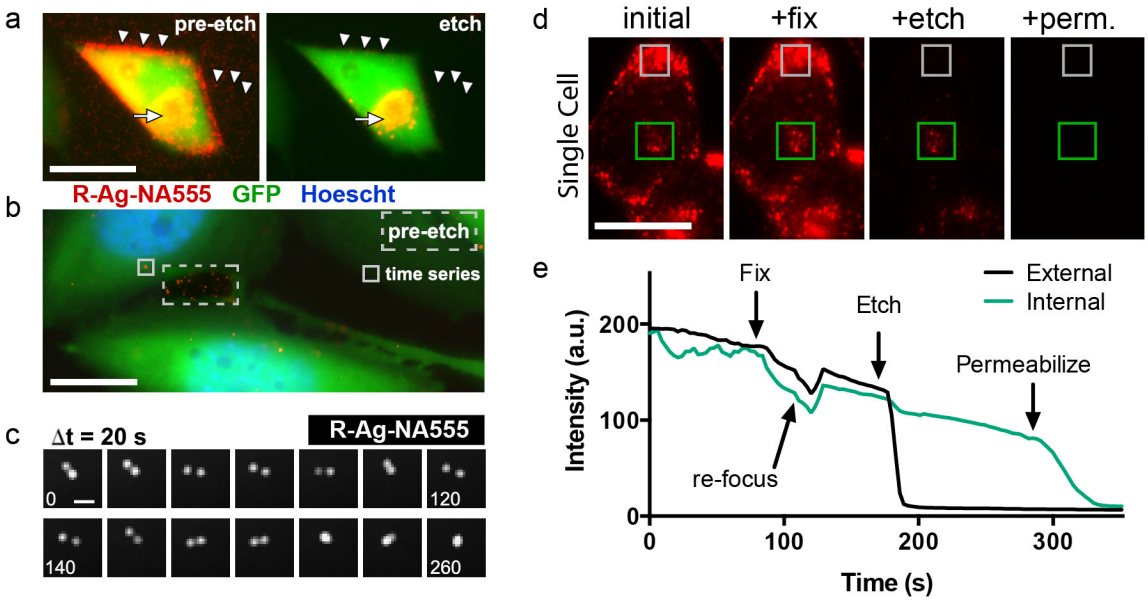

Figure 4. Tracking AgNPs within live cells

(a) Epifluorescence microscopy of GFP-expressing PC-3 cells after binding and endocytosing R-Ag-NA555. These cells express the NRP-1 receptor. R-Ag-NA555 appears red when not associated with the GFP in cells, and these were removed by etching (arrowheads). The yellow color represents cell-associated R-Ag-NA555, due to spatial overlap with the cells, indicated by the full arrow. See also Supplementary Movie S8. (b) Intracellular tracking was possible by time-lapse epifluorescence imaging when a lower amount of R-Ag-NA555 was added with shorter incubation time. This post-etch image shows only a small number of red objects survived etching, and a pre-etch image of a region outside the cells (dashed box) is overlaid to show the representative intensity from R-Ag-NA555 that had adsorbed to the substrate. A region inside the cell body (solid box) was chosen for the time series presented in c. (c) R-Ag-NA555 moved within the cell and relative to each other. Each frame advances forward by 20 s, with numbers in frames indicating the elapsed time. The two structures undergo an apparent fusion event at +220 s. (d) R-Ag-NA555 were incubated with PC-3-GFP cells and imaged during the sequential procedure of fixing (fix), etching, and permeabilization (perm.). Representative regions for R-Ag-NA555 that were internalized (green box), and a region of bound but external particles (gray box). (e) Time trace of the mean pixel intensity of the regions in d with each reagent added without washing. Rapid drops in intensity were due to etching of Ag and the gradual downward slope is due to fluorescence photobleaching. Two cells were averaged for this trace. Scale bars are 25 μm in a, 10 μm in b, 1 μm in c, 25 μm in d.

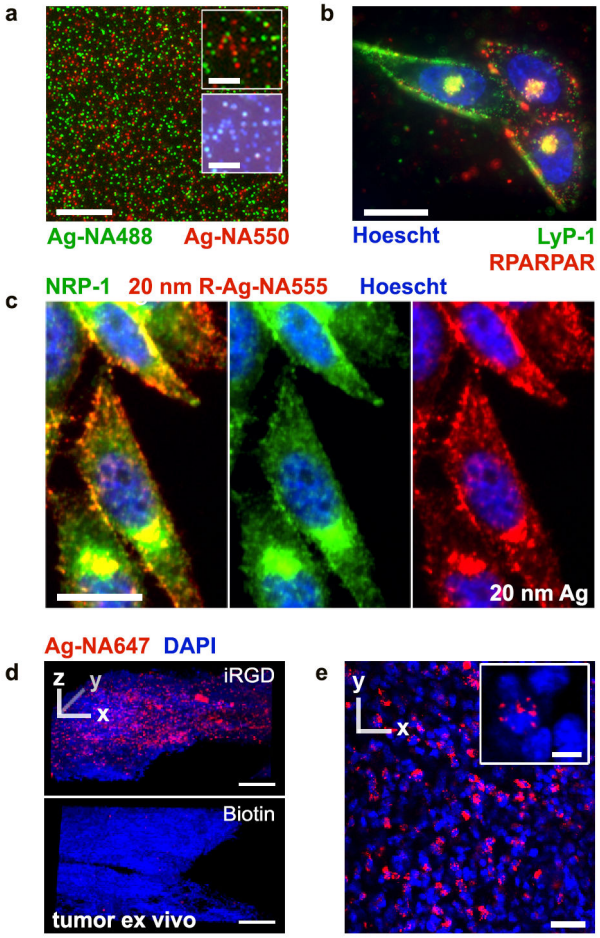

Figure 5. Distinguishing individual AgNPs of different colors, in cancer cells and tumors

(a) Microscopy analysis of a mixture of Ag-NA488 (green) and Ag-NA550 (red) on a glass slide, 20× objective. Insets show single nanoparticle detection in epifluorescence (upper) and color darkfield (lower). (b) PPC-1 cells were incubated with the mixture of green and red Ag-NA, carrying Lyp-1 and RPARPAR peptides, respectively. The difference in binding between cells reflects receptor specific binding, with colocalization in endosomes occuring near the nucleus (Hoescht, blue), 100× objective. (c) Smaller 20 nm R-Ag-NA555 (red) imaged by epifluorescence after incubation with PPC-1 cells and counterstaining with anti-NRP-1 antibody, Alexa Fluor 488 secondary antibody (green), and Hoescht. (d) Living tumor slices of 200 μm thickness were prepared from resected tumors and cultured in media. Confocal laser microscopy was performed after incubation and etching of (top) iRGD-Ag-NA647 or (bottom) biotin Ag-NA647 as a non-peptide control. Strong internalization was seen with iRGD. Z-stacks were collected through 60 μm total thickness, step size 2 μm, 20× objective. (e) 2D slice from d, top, for iRGD-Ag-NA647. Inset shows the perinuclear localization in red, 40× objective. Scale bars are 25 μm except in a-inset 5 μm, d 100 μm, and in e-inset 5 μm. DyLight 488 and 550 were used in a and b, CF555 in c, and CF647 in d.

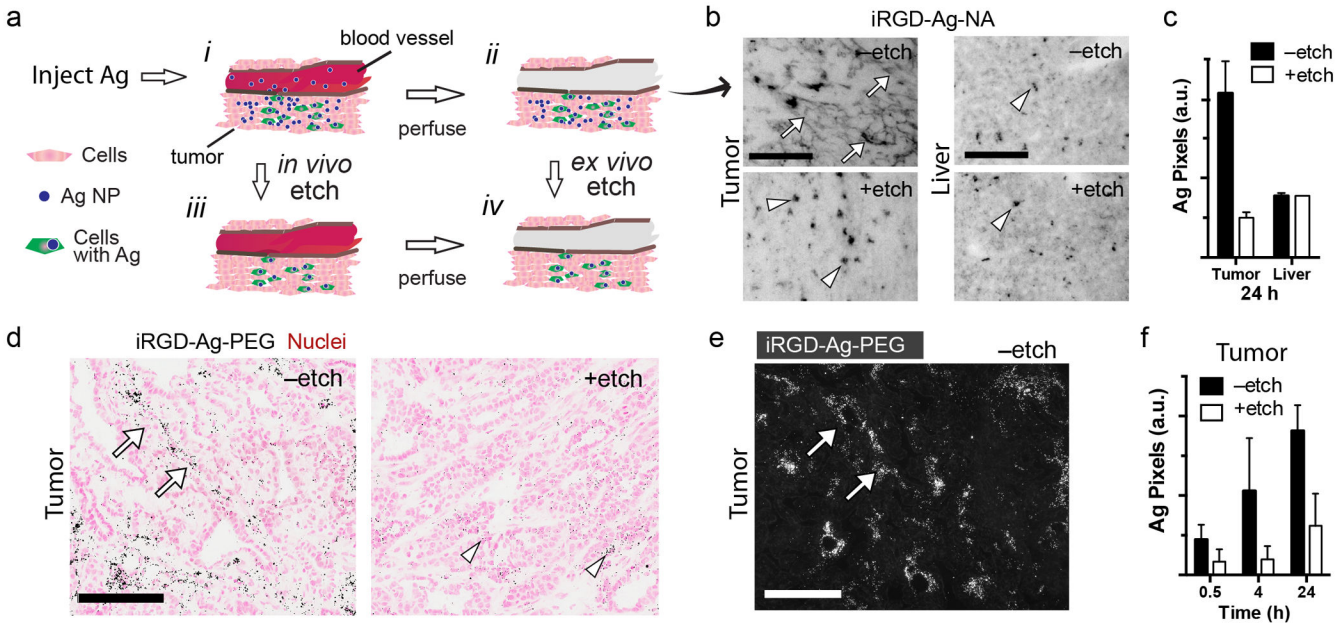

Figure 6. In vivo etching

(a) Schematic of in vivo tumor homing, ex vivo and in vivo etching. Stages are: (i) iRGD-Ag-NA homing and extravasation, (ii) tissue perfusion was followed by etching ex vivo, or instead, (iii) in vivo etching followed by perfusion, and (iv) tissue with Ag retained in cells. (b) Brightfield imaging of ex vivo 4T1 tumor and liver tissue sections are presented, −etch (upper), +etch (lower). Ag was amplified by autometallography and appeared as dark pixels. Diffuse dark pixels (full arrows) were attributed to extracellular Ag, arrowheads to endosomal Ag. (c) Samples from b were quantified for dark Ag pixels per field as a measure of iRGD-Ag-NA in the tissue. (d) In vivo etching with MMTV-PyMT tumors. Mice were perfused at 0.5, 4, or 24 h hours post injection of iRGD-Ag-PEG, and selected mice (+etch) were injected with etchant 10 min prior to perfusion. Shown are representative tumor tissue sections from 4 h –etch (left), + etch (right). (e) Darkfield imaging of Ag amplified section (4 h, –etch) shows strong signals (arrows) consistent with the pattern in brightfield, d. Note: this image has no nuclear counterstain and was taken from a separate section than d. (f) Tumor samples from d were quantified for dark Ag pixels per field, representing the amount of iRGD-Ag-PEG in the tissue for the indicated circulation times. Error bars = S.D. with N>2 randomly chosen fields per condition in c, N>4 in f. Scale bars are 100 μm in b,d,e.